Atmos. Meas. Tech. Discuss., 7, 5883–5920, 2014
www.atmos-meas-tech-discuss.net/7/5883/2014/
doi:10.5194/amtd-7-5883-2014

Atmospheric Measurement Techniques Discussions

A simple and versatile cloud-screening method for MAX-DOAS retrievals

C. Gielen[1], M. Van Roozendael[1], F. Hendrick[1], G. Pinardi[1], T. Vlemmix[2], V. De Bock[3], H. De Backer[3], C. Fayt[1], C. Hermans[1], D. Gillotay[1], and P. Wang[4]

[1]Belgian Institute for Space Aeronomy (BIRA-IASB), Brussels, Belgium
[2]Department of Geosciences and Remote Sensing, Delft University of Technology, the Netherlands
[3]Royal Meteorological Institute of Belgium, Brussels, Belgium
[4]Institute of Atmospheric Physics, Chinese Academy of Sciences, Beijing, China

Received: 25 April 2014 – Accepted: 28 May 2014 – Published: 12 June 2014

Correspondence to: C. Gielen (clio.gielen@aeronomie.be)

Published by Copernicus Publications on behalf of the European Geosciences Union.

Abstract

We present a cloud-screening method based on differential optical absorption spectroscopy (DOAS) measurements, more specifically using zenith sky spectra and O_4 differential slant-column densities (DSCDs). Using the colour index (CI), i.e. the ratio of the radiance at two wavelengths, we define different sky conditions including clear, thin clouds/polluted, fully-cloudy, and heavily polluted. We also flag the presence of broken and scattered clouds. The O_4 absorption is a good tracer for cloud-induced light-path changes and is used to detect clouds and discriminate between instances of high aerosol optical depth (AOD) and high cloud optical depth (COD).

We apply our cloud screening to MAX-DOAS (multi-axis DOAS) retrievals at three different sites with different typical meteorological conditions, more specifically suburban Beijing (39.75° N, 116.96° E), Brussels (50.78° N, 4.35° E) and Jungfraujoch (46.55° N, 7.98° E). We find that our cloud screening performs well characterizing the different sky conditions. The flags based on the colour index are able to detect changes in visibility due to aerosols and/or (scattered) clouds. The O_4-based multiple-scattering flag is able to detect optically thick clouds, and is needed to correctly identify clouds for sites with extreme aerosol pollution. Removing data taken under cloudy conditions results in a better agreement, in both correlation and slope, between the AOD retrievals and measurements from other co-located instruments.

1 Introduction

In recent years, ground-based multi-axis differential absorption spectroscopy (MAX-DOAS) has shown to be ideally suited for the retrieval of tropospheric trace gases and deriving information on aerosol properties (e.g. Hönninger et al., 2004; Wagner et al., 2004; Frieß et al., 2006; Clémer et al., 2010; Hendrick et al., 2014). These measurements are invaluable to our understanding of the physics and chemistry of the atmospheric system, and the impact on the Earth's climate.

AMTD
7, 5883–5920, 2014

MAX-DOAS retrievals of trace-gas columns and aerosol optical depths typically assume clear-sky conditions in the forward model. However, MAX-DOAS measurements are often strongly affected by clouds, leading to significant data quality degradation and larger uncertainties on the retrievals. This, in turn, strongly hinders the use of ground-based retrievals in the context of satellite validation.

In this paper we present a cloud-screening method, based on (MAX-)DOAS measurements, which aims at providing a general qualification of the sky and cloud conditions during the measurements. The data set consists of multi-year observations made at three sites with very different typical meteorological conditions, Xianghe (suburban Beijing, 39.75° N, 116.96° E), Brussels (50.78° N, 4.35° E) and the alpine station of Jungfraujoch (46.55° N, 7.98° E). We focus on 90° elevation observations since simulations show these are the most sensitive to the sky conditions. Moreover, they are independent of the azimuth angle, and are very sensitive to the temporal variability of clouds above the instrument site. The use of the zenith measurements means that the cloud-screening method is not only limited to MAX-DOAS but can also be applied to similar instruments working in the zenith mode only.

The recent paper of Wagner et al. (2013) described in detail the effect of clouds on the different quantities derived from MAX-DOAS observations, such as the radiance, colour index, O_4 absorption and the Ring effect (the filling-in of Fraunhofer lines due to inelastic scattering on atmospheric molecules). They developed a cloud-screening method based on these effects and on the comparison with clear-sky reference simulations. The method was applied to observations made during the CINDI campaign (Piters et al., 2012), where a good agreement with sky images taken from the ground was found. However, the total data set used contained data of only a limited time span (12 June 2009–15 July 2009).

Our cloud-screening method is similar to the method described in Wagner et al. (2013) but uses a simpler approach. Both methods use colour-index (CI) simulations and the temporal variability of the CI and O_4 absorption, but our method is not based on radiance or O_4 simulations and does not use information from the full MAX-DOAS

AMTD
7, 5883–5920, 2014

elevation scan but focusses only on the zenith elevation (and in lesser degree the 30° elevation). Our approach is furthermore based on a general simulation model of the colour index, which is used for all different measurement sites, thereby strongly reducing the computational cost and enhancing the general applicability of the method.

This paper shows that a simple cloud-screening method can be successfully applied to large data sets measured under a wide variety of meteorological conditions, from the extreme polluted atmosphere above Xianghe, the cloud-dominated Brussels data set, to the pristine alpine skies in Jungfraujoch.

In Sect. 2 the different MAX-DOAS instruments and the DOAS data analysis are described. In Sect. 3 the concept of the colour index and its relationship with sky and cloud conditions are presented. A description of our cloud-screening method and the definition of the cloud-screening flags can be found in Sect. 4. In Sect. 5 the results from the cloud screening at Brussels with co-located thermal infrared cloud-cover measurements are compared. Next, we apply our cloud-screening to aerosol model retrievals. A description of the radiative transfer model and co-located aerosol measurements and the resulting effect of the cloud screening on the agreement between model and measurements can be found in Sect. 6. We end with the conclusions in Sect. 7.

2 MAX-DOAS measurements

The MAX-DOAS instrument is a passive DOAS instrument that performs quasi-simultaneous measurements of scattered sunlight for a range of different elevations, from the horizon to the zenith (Hönninger et al., 2004; Platt and Stutz, 2008). This results in an enhanced sensitivity to absorbing species in the lower troposphere compared to zenith observing techniques.

AMTD
7, 5883–5920, 2014

2.1 Instrument and site description

This study focusses on MAX-DOAS measurements at three different sites with very different typical meteorological conditions, namely Brussels, Jungfraujoch and Xianghe (suburban Beijing). Xianghe is characterised by a polluted atmosphere, with episodes of extreme aerosol conditions which lead to a very low visibility. The sky over Brussels on the other hand only suffers from mild pollution, but is strongly affected by the presence of clouds. The alpine station of Jungfraujoch experiences almost no aerosol pollution but can suffer from cloudy and snowy conditions.

The instrument in Xianghe (39.75° N, 116.96° E) is located about 60 km east of Beijing and points towards the north azimuthal direction, with a 0.8° field of view. For Xianghe a full MAX-DOAS scan is comprised of 9 different elevations angles (2°, 4°, 6°, 8°, 10°, 12°, 15°, 30°, and 90°) and takes about 15 min of measurement time. This instrument has been discussed in detail in Clémer et al. (2010); Hendrick et al. (2014). It is a dual-channel instrument composed of two grating spectrometers, covering the UV (300–390 nm) and visible (400–720 nm) wavelength regions. The Xianghe MAX-DOAS instrument has been designed and assembled at the Belgian Institute for Space Aeronomy (BIRA-IASB) in Brussels, and has been continuously running since 2010.

The mini-MAX-DOAS instrument in Brussels (50.78° N, 4.35° E), has a shorter wavelength range, limited to 290–435 nm, again pointing north, with a 0.6° field of view. A full scan goes over 11 elevation angles (2°, 3°, 4°, 5°, 6°, 8°, 10°, 12°, 15°, 30°, and 90°) and requires approximately 15 min. It is a commercial system from Hoffmann Messtechnik GmbH and has been continuously running since 2011. A more detailed description of the instrument can be found in Ma et al. (2013).

The alpine station of Jungfraujoch (46.55° N, 7.98° E) is located in the Swiss Alps, at an altitude of 3570 m. A dual-channel UV (300–390 nm) and VIS (400–550 nm) MAX-DOAS instrument has been installed by BIRA-IASB and operational there since 2010. The configuration of the instrument is similar to the one in Xianghe, but it can also

AMTD
7, 5883–5920, 2014

reach negative elevation angles pointing down in the valley (−10,−8,−6,−4,−2, and 0°). However, we do not use these negative elevations in this work.

2.2 DOAS data analysis

The first step of the retrieval consists of analysing the MAX-DOAS spectra by making use of the DOAS method (Platt and Stutz, 2008). This method is developed to separate narrow-band differential absorption patterns (which can be related to specific molecules in the atmosphere) from broad-band extinction caused by Rayleigh and Mie scattering (from air molecules, aerosols and dust). The direct products of this technique are differential slant column densities (DSCDs), i.e. the integrated concentration of absorbing molecular species along the effective light path relative to the integrated concentration along the average light path of a reference spectrum. To analyse the MAX-DOAS spectra the spectral-fitting software package QDOAS is used (http://uv-vis.aeronomie.be/software/QDOAS/).

Information on aerosol characteristics, i.e. AOD and extinction profile, is obtained using O_4 DSCDs (see Sect. 6.1). This is possible since the vertical distribution of O_4 is well known and nearly constant, as it varies with the square of the O_2 monomer. Deviations of the O_4 DSCD from values representative for a clear sky are often caused by aerosols or clouds. Measurements of the O_4 DSCD can therefore be used for the retrieval of aerosols (Hönninger et al., 2004; Wagner et al., 2004; Frieß et al., 2006). These DSCDs are retrieved in the UV (338–370 nm) for Brussels, Jungfraujoch and Xianghe, and in the VIS for Xianghe and Jungfraujoch (425–490 nm), using the O_4 cross sections from Hermans et al. (2003). These wavelength ranges are the most sensitive to O_4 absorption (Roscoe et al., 2010), and have minimal interference from other absorbing species. Other trace gases used for the fitting include NO_2, O_3, H_2O, HCHO, and BrO, along with a Ring spectrum. For the observed broad-band extinction a fifth-order polynomial is used. A detailed description of the QDOAS setting for aerosol retrievals can be found in Clémer et al. (2010).

AMTD
7, 5883–5920, 2014

3 The colour index

To characterize the sky conditions at the different measurement sites we develop a cloud-screening method based on two different measured quantities: the colour index (CI) of the sky and the O_4 DSCDs. The CI is defined as the ratio of the intensity of a measured spectrum at two wavelengths, and gives information on the observed colour of the sky. Since the sky colour changes from blue during clear skies to white/gray when clouds or aerosols are present, we can use the CI to qualify the sky condition.

The CI for Xianghe, Brussels, and Jungfraujoch are defined as I_{405}/I_{670}, I_{347}/I_{420}, and I_{405}/I_{560} respectively, with I_x the median intensity over the $[x-5\,\text{nm}, x+5\,\text{nm}]$ wavelength range. The wavelength regions were chosen to obtain the largest spectral contrast and avoid the influence of strong atmospheric spectral features.

As can be seen in Fig. 1, the CI shows a clear pattern depending on the observed meteorological conditions. For clear skies the CI values are high, due to the wavelength dependence of Rayleigh scattering, and they decrease with increasing aerosol load (Fig. 1a) since scattering on aerosol and cloud particles is less wavelength dependent. We also see a clear separation between the different elevation angles of the observations. The highest CI values can be found for spectra with the highest elevation angles, whereas low elevation angles show lower values and spread. In the case of an extreme aerosol load or full cloud cover, the CI values are all clustered around a constant value (Fig. 1b–c). In the case of broken or scattered clouds, the CI shows a very variable temporal behaviour (Fig. 1d).

Simulations of the CI corroborate the observed decrease of the CI in the presence of clouds and aerosols, as can be seen in Fig. 2. These simulations were made with the DAK (doubling-adding KNMI code) radiative transfer model (Stammes et al., 1989; Stammes, 2001, http://www.knmi.nl/~stammes/DAK/Manual_DAKver312.pdf) under varying aerosol and cloud optical depths, and varying parameters such as wavelength, elevation, SZA and azimuth angle. The cloud base height was set at 1 km

AMTD
7, 5883–5920, 2014

and atmospheric Rayleigh scattering and ozone absorption were included. These simulations also show that it is very difficult to distinguish between aerosols and clouds using only CI information. For this reason also information from the observed O_4 DSCDs will be used, which will be discussed in a later section (Sect. 4.3).

For the rest of this study only the CI derived from zenith observations is used, as the CI derived from spectra with low elevations angles shows a very narrow spread, making it difficult to distinguish between the different parameters. This effect can be clearly seen in Fig. 2, where the different simulations reach similar values for lower elevation angles. These simulations furthermore show that the same problem of overlapping simulations occurs for observations taken at SZA > 85°. For this reason we also eliminate these data from our study.

The resulting calculated zenith CI values for the full Xianghe, Brussels and Jungfraujoch data sets can be found in Fig. 3. All sites show a frequency distribution with a clear peak at the lowest CI values, corresponding to observations taken under non-clear sky conditions. For Junchfraujoch we see a more bimodal distribution, where the small peak at higher CI values corresponds to a larger frequency of clear days, compared to the other sites. The differences in the observed CI values between the different sites are due to the different wavelength ranges used for the CI calculation and the differences in instrumental response. It is important to investigate the behaviour of the CI over time to spot variations in the CI which are due to instrumental issues, such as a shift in instrumental response after technical difficulties, changes in set-up, or instrument degradation. If clear CI variations are spotted that can be linked to instrumental issues, it is important to correct for this.

4 The cloud-screening method

To characterize the sky conditions we define 3 different flags: the sky flag, the broken-cloud flag, and the multiple-scattering flag. The sky flag defines the general sky conditions in terms of visibility; i.e. clear, mediocre, and bad. This flag does not distinguish

AMTD
7, 5883–5920, 2014

between a visibility reduction due to clouds or aerosols. The broken-cloud flag denotes the presence of broken or scattered clouds in the line-of-sight. The third flag, which is based on the O_4 DSCDs and not the CI, marks the presence of enhanced multiple scattering in the line-of-sight, and thus the presence of thick clouds.

4.1 The sky flag

For the sky flag we define 3 regions of CI values which are linked to 3 general sky conditions in terms of visibility; i.e. clear, mediocre, and bad. To do this the calculated CI values are normalized between 0 and 1, to get rid of wavelength and instrumental effects on the CI between the different measurement sites. This can only be done if enough data are available to have observations during both very clear and low-visibility sky conditions, which allows the determination of the minimum and maximum CI values.

To constrain the 3 regions, the full set of normalized CI values is compared with a grid of pre-calculated CI simulations, which we scale to give the best match with the observed spread in CI. For this the plane-parallel DAK simulations described in Sect. 3 are used, which are calculated for a range of different wavelengths, corresponding to the ones used for the CI calculation at the different sites. We do not fine-tune other model parameters such as surface albedo to the different site characteristics to minimise the computational effort. The simulations are scaled in such a way that the peak of the normalized CI frequency distribution corresponds to the clustering of simulations with high aerosol and/or cloud optical depth (AOD/COD), and so that the simulation with the lowest simulated aerosol optical depth (AOD = 0.05) follows the top of the normalized measured CI values. Additional AOD information from co-located instruments such as a cimel sun photometer (Holben et al., 2001), Brewer spectrophotometer (De Bock et al., 2010), or solar irradiance instruments (Nyeki et al., 2012) is used to validate the procedure and make small adjustments in the scaling. As can be seen in Fig. 4, the distribution of scaled CI simulations corresponds well to the observed CI values and measured AOD values.

AMTD
7, 5883–5920, 2014

We then arbitrarily take the scaled simulation made with AOD = 0.15 and COD = 0.0 (green-diamond line in Fig. 4) as the limit to separate the "good" and "mediocre" region: CI values above this curve are flagged as made under "good" visibility conditions. To separate between the "mediocre" and "bad" regions we define a horizontal line in such a way that the peak of the frequency distribution falls in the "bad" region. The resulting "good", "mediocre", and "bad" regions can be seen as, respectively, the green, orange, and red regions in Fig. 5.

These regions correspond to different meteorological conditions. Data flagged as "good" is taken under relatively clear conditions, i.e. very low aerosol and cloud optical depth. "Mediocre" data represents data under sky conditions with slightly decreased visibility, i.e. thin clouds and/or moderate aerosol pollution. Data with a "bad" flag points to the presence of thick clouds and/or extreme aerosol conditions.

4.2 The broken-cloud flag

To determine the presence of broken or scattered clouds in the line-of-sight of measurement, the temporal variability of the CI is studied. As could already be seen in Fig. 1, the CI remains very stable for clear skies, skies with aerosol pollution, and skies with a full cloud cover, but in the presence of scattered clouds, the CI shows large drops in value when a cloud passes over.

To quantify this we model the observed CI values for each day with a double-sine function of the form $f(x) = a + b\sin(cx - d) + e\sin(fx - g)$. Outliers are then identified as those data points with $|(\text{CI-model})| > C$, with $C = 0.2$ for Xianghe, $C = 0.05$ for Brussels, and $C = 0.1$ for Jungfraujoch. These outliers are flagged as observations made under scattered/broken-cloud conditions. Examples of this modelling and outlier determination can be found in Fig. 6.

Note that this flag does not give any information about the presence of a full cloud cover, since this will not give rise to strong temporal variation in the CI values. The influence of aerosol variability on the temporal variation of the CI typically gives rise

AMTD
7, 5883–5920, 2014

to a more smooth increase or decrease, and will not give rise to the strong temporal jumps seen for cloud contamination.

4.3 The multiple-scattering flag

As discussed in the previous sections, the CI alone is not enough to distinguish between the presence of visibility reduction due to clouds or to aerosols. To resolve this problem we also define an additional constraint based on the measured O_4 DSCDs, which provide information on the effective light path of scattered photons. Clouds can have an increasing or decreasing effect on the O_4 DSCD value, with respect to clear sky conditions. The first typically occurs for optically thick clouds, due to enhanced multiple scattering in the cloud layer. Optically thin clouds at high altitudes can also lead to an increase, but only for measurements under low elevation angles. Thin clouds at low altitudes tend to decrease the O_4 DSCDs at all elevation angles (Wagner et al., 2011). An increase in aerosol load will also effect the O_4 DSCDs, and will lead to a decrease in observed spread for the different elevation angles, as can clearly be seen in Fig. 1a.

Since both clouds and aerosols can thus have a very complex effect on the O_4 absorption, which can only be investigated in detail by comparing with radiative transfer models (as done in Wagner et al., 2013), we opt to only study the temporal variation of the measured O_4 DSCDs. Strong temporal variability due to enhanced multiple scattering commonly occurs in optically thick clouds, and is seen less for high aerosol optical depth, as illustrated by Fig. 1.

To study the temporal variability a similar procedure as for the detection of broken clouds is applied. Since we are not interested in slow and smooth changes in O_4 absorption, such as the observed diurnal trend, the DSCD measured at zenith is subtracted from the DSCDs at lower elevation angles α. This technique is commonly used in MAX-DOAS retrieval studies (e.g. Clémer et al., 2010; Hendrick et al., 2014), as it effectively removes the (negligible) stratospheric contribution to the O_4 absorption (Hönninger et al., 2004). Here, it has the advantage of removing the very strong diurnal trend, which hinders our modelling and outlier detection.

AMTD
7, 5883–5920, 2014

We then again model the resulting O_4 (α–90°) DSCDs with a double-sine function, and define an outlier as points with $|(O_4\text{-model})/\text{model}| > 0.2$. This flag can be defined for measurements at each elevation angle, but here we will focus further only on the 30–90° elevation scan, as the 30° elevation is closest to zenith and thus will encounter the lowest temporal cloud variation. In the case of zenith-pointing DOAS instruments, one could use only the zenith O_4 data, but then a model curve suited to fit the strong diurnal variation needs to be chosen.

A good agreement is found between the O_4-based flag and information derived from the CI-based flags. Both types of flags can be used to mark cloudy data, i.e. data with enhanced multiple scattering on the one hand and data with a "bad" sky flag or broken-cloud flag on the other. Ideally, the same data points should be flagged using the two flag types. However, the multiple-scattering flag will be most sensitive to clouds with a high optical depth, whereas the colour index is also sensitive to clouds with a lower cloud optical depth, as even such clouds quickly change the observed sky colour.

For Brussels this indeed seems to be the case and a good agreement of 85 % is found, for Jungfraujoch however only about 60 % of points get marked as cloudy by both flag types. The Xianghe data set shows the limitations of cloud screening using only the CI flags: when using the CI flags 20 % more data is marked as cloudy in comparison to the multiple-scattering O_4 flag. This is due to the fact that events of high aerosol optical depth are wrongly flagged as cloudy. For sites where such events occur regularly, the multiple scattering flag seems to be a better choice to detect thick clouds. However, since the multiple-scattering flag requires a much larger computational effort compared to the CI flags and it adds little additional information for low or mild aerosol pollution, we opt not to use it for such sites. A comparison between the effect of the different flags on measurements can be found in Sect. 6.

AMTD
7, 5883–5920, 2014

5 Comparison with infrared cloud-cover measurements

In order to validate the previously defined flags, the cloud-screening results for Brussels are compared with thermal infrared cloud-cover measurements. The Brussels site has access to an infrared pyrometer, which determines the total cloud cover fraction based on temperature data over a field of view of 6° (Gillotay et al., 2001). The method works well to describe most cloudy conditions, with the exception of cirrus clouds with variable emissivity. The total cloud-cover fraction is defined as the ratio between the observed cloudy solid angle elements and clear-sky elements.

In Fig. 7 the total cloud-cover fraction values for an example day can be seen, where we colour-marked our different CI flagging results. High cloud-cover fractions are systematically flagged with a "bad" sky flag, whereas low cloud-cover data correspond to "good/mediocre" sky flags. These results are summarised in Fig. 8 where the distribution of cloud-cover values for the full Brussels data set (~ 2.5 years) is given, together with the distribution of points with corresponding sky flags. In the bottom plot the fraction of our sky flag results over the cloud-cover values are shown. Data with high cloud-cover fractions ($> 60\,\%$) are generally flagged as "bad" by our cloud screening, whereas $\gtrsim 80\,\%$ points with a cloud-cover fraction $< 20\,\%$ are flagged as "good/mediocre with no broken clouds".

The same exercise was performed for the multiple-scattering flag, and we again find that data with a high cloud-cover fractions are typically flagged as having a multiple-scattering. This can again be seen in Fig. 8, where the blue line denotes the distribution of the MS flag over the cloud-cover percentages. We do find that compared to the flags derived from the CI, more data with low cloud-cover values are flagged as having multiple scattering, i.e. being cloudy.

This shows that there is a good agreement between our cloud screening and the cloud-cover determination. One has to take into account that the field-of-view of the thermal infrared instrument is significantly larger than that of the MAX-DOAS, and thus that different areas of the sky are measured. Also, the value of our sky flag does not only

AMTD
7, 5883–5920, 2014

depends on the presence of clouds, but also on the aerosol content. This means that cloud-free measurements can still be flagged as "mediocre" (or even "bad") if aerosols are present.

6 Application to aerosol model retrievals

With the flags defined in the previous section we proceed to define a cloud-screening procedure for our MAX-DOAS retrievals. For this particular study we are interested in the aerosol load of the atmosphere, which means data too strongly affected by clouds needs to be removed, but measurements made under polluted conditions should be retained.

For this reason we investigate data with a sky flag of either "good" or "mediocre", since a sky flag of "bad" is most commonly found for fully-cloudy conditions. To remove data which are affected by scattered or broken clouds, we only keep data which are not flagged in the broken-cloud screening. This effectively removes all the cloud-contaminated data from our data sets. However, it also removes data under extreme aerosol conditions, as is often found in Xianghe, as those measurements will also be flagged as "bad" in the sky-flag determination. To resolve this issue, we use the multiple-scattering flag to differentiate between measurements made under conditions with either high AOD or high COD.

6.1 AOD model retrievals and measurements

To study the effect of our cloud-screening method, AOD values retrieved by MAX-DOAS are compared to co-located AOD measurements. For Xianghe and Brussels we use AERONET Level 1.5 data, and for the Brussels site we extend the comparison with co-located Brewer spectrophotometer measurements at 340 nm. A detailed description of the Brewer spectrophotometer instrument and measurements can be found in De Bock et al. (2010). The measured cimel and Brewer AOD values are then interpolated to

AMTD
7, 5883–5920, 2014

360 and 477 nm if needed, using the Ångström coefficients as provided by AERONET (Holben et al., 2001). At Jungfaujoch no AERONET instrument is available, so we used AOD values as measured by the Precision Filter Radiometer Network (Nyeki et al., 2012) in the context of the Global Atmosphere Watch – World Data Center for Aerosol (GAW-WDCA) programme of the World Meteorological Organization (WMO) (ebas.nilu.no).

For the MAX-DOAS aerosol retrievals the bePRO radiative transfer code (Clémer et al., 2010) is used, which is an inversion algorithm based on the optimal estimation method (Rodgers, 2000, OEM). The model uses the observed MAX-DOAS O_4 DSCDs to derive the vertical profiles of the aerosol extinction at different wavelengths. For Xianghe and Jungfraujoch, we focus on the 360 and 477 nm wavelengths, whereas for Brussels we only have access to the 360 nm wavelength due to the shorter instrumental range. A detailed description of the bePRO algorithm and parameters can be found in Clémer et al. (2010). It is found that the model is most sensitive to aerosols close to the surface, below 1 km, and typically contains about 1–2 pieces of independent information (DFS, degrees of freedom for signal). Only those results where the retrieved O_4 DSCDs have an RMS < 50 % compared to the measured DSCDs are kept for the further study, since high RMS values typically points to a failure of the model during the retrieval process. For Jungfraujoch we use a more strict cut-off value of RMS < 30 % since we found that our modelling was less successful and stable for this data set.

6.2 Impact on aerosol retrievals

We perform the cloud screening by defining data as cloudy if: the sky flag is "bad" or it has a broken-cloud flag when using the CI-based flags, or it has a multiple-scattering flag when using the O_4-based flag. These constraints generally correctly flag the presence of thick clouds, but are less reliable when thin clouds are present, as the discrimination between thin clouds and low/mild aerosol pollution is not straightforward.

The results of our AOD retrievals and cloud screening can be found in Fig. 9 and the online supplementary material. In these figures the AERONET AOD values (black) and

AMTD
7, 5883–5920, 2014

the cloud-screened bePRO retrievals are shown, colour-coded with the different flag values. A removal of data with evidence for the presence of clouds, be it either based on the sky and broken-cloud flag or the multiple-scattering flag, results in a much better agreement with the AOD measurements and retrievals.

For the Xianghe data set it is also clear that a cloud screening based on the colour index alone, i.e. the sky and broken-cloud flag, often removes data under extreme aerosol conditions. When using the CI flags, about 55 % of data is removed, whereas the O_4-based flag only removes about 40 % of the data. Additional information from the O_4 DSCDs, i.e. the multiple-scattering flag, is needed to make sure we can differentiate between high AOD and high COD. This problem does not arise for Brussels and Jungfraujoch where a similar amount of data is flagged as cloudy by both methods, since here the AOD typically does not reach values above 1.5. It is also clear from Fig. 9 that a correct broken-cloud identification is much more important at the Brussels site, where clouds contaminate over 60 % of the data. The Jungfraujoch data set clearly shows the low aerosol levels of the alpine site (AOD < 0.2), with significantly less cloudy conditions (~ 50 %) compared to Brussels. An overview of the statistics of data removal by the cloud-screening method can be found in Table 1.

Correlation plots between our retrievals and co-located AOD measurements (AERONET/Brewer/solar irradiance spectra) can be found in Fig. 10. For the correlation study we averaged our retrievals in time steps of 0.2 hour. Averages were given a "bad" sky flag if ≥ 50 % of individual points had a "bad" sky flag, and a broken-cloud flag if ≥ 20 % of points had a broken-cloud flag. For the multiple-scattering flag we flagged the averages if more than one data point was flagged.

One has to note that the AOD measurements (AERONET, Brewer, cimel) themselves typically only operate when direct-sun observations can be made and have already undergone a basic cloud screening, which effectively removes a large part of data to use in the correlation study. However, we do find that data for which no measurements are available are generally flagged by our method as cloudy, showing the coherence between our cloud screening and that of the other instruments. Exceptions occur when

AMTD
7, 5883–5920, 2014

these instruments are not working due to instrumental issues. For Xianghe, about 25 % of points with coincident AERONET data for the correlation study remain when averaging over 0.2 hour. For Brussels and Jungfraujoch this is less than 10 %. Another note of caution is that the MAX-DOAS and other AOD-measuring instruments have different viewing directions, and might thus trace regions with slightly different cloud and aerosol characteristics.

The correlation plots in Fig. 10 show the linear regression results using only the CI information (green/orange crosses) and the results using only the O_4 DSCD multiple-scattering information (blue diamonds). As already mentioned above, without the multiple-scattering flag from O_4 absorption we remove non-cloudy data under extreme aerosol conditions, which is especially important for the Xianghe data set.

For the Xianghe data set we find high correlation coefficients R, already for the non-cloud-screened data. For both 360 and 477 nm we have a correlation value of $R = 0.93$, and also the linear regression slopes S are very close to $S = 1$. For both wavelengths the cloud screening based on the CI slightly decreases the correlation and slope, with correlation values changing from $R = 0.93$ to $R = 0.91$–0.92. We do see a difference between the two wavelengths: at 360 nm our model seems to overestimate the AOD in comparison to AERONET, whereas the opposite occurs at 477 nm. Applying the cloud screening does improve the slope at 477 nm (from $S = 1.17$ tot $S = 1.01$), but worsens the slope at 360 nm (from 0.96 to $S = 0.88$). This difference in slopes for different wavelengths was already found for a similar study of MAX-DOAS aerosol bePRO retrievals (Clémer et al., 2010) and could possibly be due to fitting difficulties during the DOAS retrievals, or uncertainties on the aerosol phase function used in the bePRO model.

For both wavelengths it can be seen that a cloud screening using the multiple-scattering flag improves the observed correlation slightly. It is clear that this method includes an area of high AOD values which were not covered using only the CI-based cloud screening, and that for sites that experience high AOD levels the CI (alone) is not enough for a correct cloud detection.

AMTD
7, 5883–5920, 2014

For Brussels we find much lower correlation values between our results and AERONET/Brewer data. Without cloud screening, the correlation coefficient has a value of $R = 0.66$. When we remove data with a "bad" sky flag, the correlation coefficient increases to $R = 0.74$, and it increases even more when we also remove data contaminated by broken clouds, reaching a value of $R = 0.80$. Applying the cloud screening also changes the observed slope from $S = 0.75$ to $S = 0.96$ for the 0.2 h averaged time step. However, we find that even though the O_4-based cloud screening improves the correlation compared to the non-cloud-screened data, it does not give as good R values as the CI-based cloud screening.

The extremely low AOD values for Jungfraujoch make it difficult to comment on the agreement between the modelled AOD values and co-located GAW-WDCA measurements, as most of the points are clustered around AOD = 0.02. Our bePRO retrievals in some cases strongly overestimate the AOD, which screws the observed correlation and slope to extreme values of $R = 0.04$ and $S = 0$. Applying the CI-based cloud screening, which removes about 30 % of data points, does not improve the retrieved correlation. We find that the O_4-based cloud screening removes a similar amount of data points and only slightly improves the correlation. However, it is clear that the intrinsic uncertainties of the bePRO retrievals are too big in the case of very low AOD values to make strong conclusions on the observed correlations.

We conclude that for the Brussels and Jungfraujoch sites, it is sufficient to base the cloud screening on information from the colour index alone, whereas for Xianghe, additional information from O_4 DSCDs is invaluable for a correct cloud identification.

7 Conclusions

We present a cloud-screening method for MAX-DOAS measurements to qualify the sky and cloud conditions. The method is based on the colour index (CI) and on O_4 DSCD retrievals. We focus on observations made at zenith elevations, which means the method is not only limited to MAX-DOAS instruments, but can also be applied

AMTD
7, 5883–5920, 2014

to traditional zenith-sky DOAS measurements. The cloud screening based on the CI has the advantage that it only needs two relative intensities, which can be measured by different types of non-DOAS instruments. The method based on the O_4 DSCDs has the advantage of giving better results for sites experiencing extreme aerosol concentrations and does not rely on simulations.

We use the calculated CI values combined with CI simulations to characterise the general sky conditions, in the form of the sky flag, and define three distinct regions corresponding to clear sky, slightly decreased visibility (thin clouds/aerosols), and strongly decreased visibility (thick clouds/extreme aerosols). At this point no distinction is made between a visibility decrease due to clouds and/or aerosols. The temporal variation of the CI is used to identify the presence of broken or scattered clouds, and is given by the broken-cloud flag. The third flag, the multiple-scattering flag, is based on the O_4 DSCDs and it detects (optically thick) clouds by tracing enhanced multiple scattering.

The values of the CI not only depend on the sky conditions, but also on the instrument characteristics and wavelength settings, and it is thus impossible to define a standardised method that is valid for all different measurement sites. For this reason we scale the calculated observed CI values to CI simulations. The drawback to this approach is that a substantial amount of data, which span observations under both good and bad sky conditions, is needed to verify the applied scaling. Additional data, such as from cimel or Brewer instruments, can help resolve this issue. Ideally, all MAX-DOAS instruments should have well-defined and frequent calibration procedures, to eliminate the instrumental effects and allow for a direct comparison of the CI.

We applied our cloud-screening method to three large multi-year data sets of MAX-DOAS measurements in suburban and rural regions, namely Xianghe, Brussels, and Jungfraujoch. All sites are characterised by different typical sky conditions: Xianghe is generally strongly polluted, with days of extreme aerosol loads. Brussels on the other hand shows only mild aerosol pollution but suffers from year-round cloudy conditions. The alpine station of Jungfraujoch shows very low aerosol pollution levels and average cloud pollution.

AMTD
7, 5883–5920, 2014

We find that our method works very well to identify observations made under cloudy conditions using only the colour index. In the case of Xianghe the method is even capable of discriminating between high AOD and high COD by using additional information from the O_4 DSCDs. When we apply the cloud filter to our aerosol retrievals we find an improvement in the agreement with other co-located measurements, such as from cimel and Brewer instruments, both in correlation and slope.

The Supplement related to this article is available online at doi:10.5194/amtd-7-5883-2014-supplement.

Acknowledgements. This research was financially supported at IASB-BIRA by the Belgian Federal Science Policy Office, Brussels (AGACC-II project SD/CS/07A), the EU 7th Framework Programme projects NORS (contract 284421), and the ESA CEOS Intercalibration project (ESA/ESRIN Contract 22202/09/I-EC). P. Stammes (KNMI) is acknowledged for providing us the DAK code.

References

Clémer, K., Van Roozendael, M., Fayt, C., Hendrick, F., Hermans, C., Pinardi, G., Spurr, R., Wang, P., and De Mazière, M.: Multiple wavelength retrieval of tropospheric aerosol optical properties from MAXDOAS measurements in Beijing, Atmos. Meas. Tech., 3, 863–878, doi:10.5194/amt-3-863-2010, 2010. 5884, 5887, 5888, 5893, 5897, 5899

De Bock, V., De Backer, H., Mangold, A., and Delcloo, A.: Aerosol Optical Depth measurements at 340 nm with a Brewer spectrophotometer and comparison with Cimel sunphotometer observations at Uccle, Belgium, Atmos. Meas. Tech., 3, 1577–1588, doi:10.5194/amt-3-1577-2010, 2010. 5891, 5896

Frieß, U., Monks, P. S., Remedios, J. J., Rozanov, A., Sinreich, R., Wagner, T., and Platt, U.: MAX-DOAS O_4 measurements: a new technique to derive information on atmospheric aerosols: 2. Modeling studies, J. Geophys. Res.-Atmos., 111, D14203, doi:10.1029/2005JD006618, 2006. 5884, 5888

AMTD
7, 5883–5920, 2014

Gillotay, D., Besnard, T., and Zanghi, F.: A systematic approach of the cloud cover by thermic infrared measurements, Proceedings of 18th Conference on Weather Analysis and Forecasting, Fort Lauderdale, Fl, USA, 30 July–2 August 2001, 292–295, 2001. 5895

Hendrick, F., Müller, J.-F., Clémer, K., Wang, P., De Mazière, M., Fayt, C., Gielen, C., Hermans, C., Ma, J. Z., Pinardi, G., Stavrakou, T., Vlemmix, T., and Van Roozendael, M.: Four years of ground-based MAX-DOAS observations of HONO and NO_2 in the Beijing area, Atmos. Chem. Phys., 14, 765–781, doi:10.5194/acp-14-765-2014, 2014. 5884, 5887, 5893

Hermans, C., Vandaele, A., Fally, S., Carleer, M., Colin, R., Coquart, B., Jenouvrier, A., and Merienne, M.-F.: Absorption cross-section of the collision-induced bands of oxygen from the UV to the NIR, vol. 27 of NATO Science Series, Springer, The Netherlands, doi:10.1007/978-94-010-0025-3_16, 2003. 5888

Holben, B. N., Tanré, D., Smirnov, A., Eck, T. F., Slutsker, I., Abuhassan, N., Newcomb, W. W., Schafer, J. S., Chatenet, B., Lavenu, F., Kaufman, Y. J., Castle, J. V., Setzer, A., Markham, B., Clark, D., Frouin, R., Halthore, R., Karneli, A., O'Neill, N. T., Pietras, C., Pinker, R. T., Voss, K., and Zibordi, G.: An emerging ground-based aerosol climatology: aerosol optical depth from AERONET, J. Geophys. Res.-Atmos., 106, 12067, doi:10.1029/2001JD900014, 2001. 5891, 5897

Hönninger, G., von Friedeburg, C., and Platt, U.: Multi axis differential optical absorption spectroscopy (MAX-DOAS), Atmos. Chem. Phys., 4, 231–254, doi:10.5194/acp-4-231-2004, 2004. 5884, 5886, 5888, 5893

Ma, J. Z., Beirle, S., Jin, J. L., Shaiganfar, R., Yan, P., and Wagner, T.: Tropospheric NO_2 vertical column densities over Beijing: results of the first three years of ground-based MAX-DOAS measurements (2008–2011) and satellite validation, Atmos. Chem. Phys., 13, 1547–1567, doi:10.5194/acp-13-1547-2013, 2013. 5887

Nyeki, S., Halios, C. H., Baum, W., Eleftheriadis, K., Flentje, H., Gröbner, J., Vuilleumier, L., and Wehrli, C.: Ground-based aerosol optical depth trends at three high-altitude sites in Switzerland and southern Germany from 1995 to 2010, J. Geophys. Res.-Atmos., 117, D18202, doi:10.1029/2012JD017493, 2012. 5891, 5897

Piters, A. J. M., Boersma, K. F., Kroon, M., Hains, J. C., Van Roozendael, M., Wittrock, F., Abuhassan, N., Adams, C., Akrami, M., Allaart, M. A. F., Apituley, A., Beirle, S., Bergwerff, J. B., Berkhout, A. J. C., Brunner, D., Cede, A., Chong, J., Clémer, K., Fayt, C., Frieß, U., Gast, L. F. L., Gil-Ojeda, M., Goutail, F., Graves, R., Griesfeller, A., Großmann, K., Hemerijckx, G., Hendrick, F., Henzing, B., Herman, J., Hermans, C., Hoexum, M., van der Hoff, G. R.,

AMTD
7, 5883–5920, 2014

Irie, H., Johnston, P. V., Kanaya, Y., Kim, Y. J., Klein Baltink, H., Kreher, K., de Leeuw, G., Leigh, R., Merlaud, A., Moerman, M. M., Monks, P. S., Mount, G. H., Navarro-Comas, M., Oetjen, H., Pazmino, A., Perez-Camacho, M., Peters, E., du Piesanie, A., Pinardi, G., Puentedura, O., Richter, A., Roscoe, H. K., Schönhardt, A., Schwarzenbach, B., Shaiganfar, R., Sluis, W., Spinei, E., Stolk, A. P., Strong, K., Swart, D. P. J., Takashima, H., Vlemmix, T., Vrekoussis, M., Wagner, T., Whyte, C., Wilson, K. M., Yela, M., Yilmaz, S., Zieger, P., and Zhou, Y.: The Cabauw Intercomparison campaign for Nitrogen Dioxide measuring Instruments (CINDI): design, execution, and early results, Atmos. Meas. Tech., 5, 457–485, doi:10.5194/amt-5-457-2012, 2012. 5885

Platt, U. and Stutz, J.: Differential Optical Absorption Spectroscopy, Springer-Verlag, Berlin, 2008. 5886, 5888

Rodgers, C. D.: Inverse Methods for Atmospheric Sounding – Theory and Practice, Series: Series on Atmospheric Oceanic and Planetary Physics, edited by: Rodgers C. D., World Scientific Publishing Co. Pte. Ltd., vol. 2, 2, Singapore, 2000. 5897

Roscoe, H. K., Van Roozendael, M., Fayt, C., du Piesanie, A., Abuhassan, N., Adams, C., Akrami, M., Cede, A., Chong, J., Clémer, K., Friess, U., Gil Ojeda, M., Goutail, F., Graves, R., Griesfeller, A., Grossmann, K., Hemerijckx, G., Hendrick, F., Herman, J., Hermans, C., Irie, H., Johnston, P. V., Kanaya, Y., Kreher, K., Leigh, R., Merlaud, A., Mount, G. H., Navarro, M., Oetjen, H., Pazmino, A., Perez-Camacho, M., Peters, E., Pinardi, G., Puentedura, O., Richter, A., Schönhardt, A., Shaiganfar, R., Spinei, E., Strong, K., Takashima, H., Vlemmix, T., Vrekoussis, M., Wagner, T., Wittrock, F., Yela, M., Yilmaz, S., Boersma, F., Hains, J., Kroon, M., Piters, A., and Kim, Y. J.: Intercomparison of slant column measurements of NO_2 and O_4 by MAX-DOAS and zenith-sky UV and visible spectrometers, Atmos. Meas. Tech., 3, 1629–1646, doi:10.5194/amt-3-1629-2010, 2010. 5888

Stammes, P.: Spectral radiance modelling in the UV-visible range, Proceedings IRS-2000: Current Problems in Atmospheric Radiation, edited by: Smith, W. L. and Timofeyev, Y. M., A. Deepak Publ., Hampton, 181–184, 2001. 5889, 5909

Stammes, P., de Haan, J. F., and Hovenier, J. W.: The polarized internal radiation field of a planetary atmosphere, Astron. Astrophys., 225, 239–259, 1989. 5889

Wagner, T., Dix, B., Friedeburg, C. v., Frieß, U., Sanghavi, S., Sinreich, R., and Platt, U.: MAX-DOAS O4 measurements: a new technique to derive information on atmospheric aerosols, principles and information content, J. Geophys. Res., 109, D22205, doi:10.1029/2004JD004904, 2004. 5884, 5888

AMTD
7, 5883–5920, 2014

Wagner, T., Beirle, S., Brauers, T., Deutschmann, T., Frieß, U., Hak, C., Halla, J. D., Heue, K. P., Junkermann, W., Li, X., Platt, U., and Pundt-Gruber, I.: Inversion of tropospheric profiles of aerosol extinction and HCHO and NO_2 mixing ratios from MAX-DOAS observations in Milano during the summer of 2003 and comparison with independent data sets, Atmos. Meas. Tech., 4, 2685–2715, doi:10.5194/amt-4-2685-2011, 2011. 5893

Wagner, T., Apituley, A., Beirle, S., Dörner, S., Friess, U., Remmers, J., and Shaiganfar, R.: Cloud detection and classification based on MAX-DOAS observations, Atmos. Meas. Tech., 7, 1289–1320, doi:10.5194/amt-7-1289-2014, 2014. 5885, 5893

AMTD
7, 5883–5920, 2014

Table 1. Overview of the number of retrieval points removed by the cloud-screening procedure. The first column shows the respective site and wavelength, the second column gives the total number of points before cloud-screening, the third columns provides the percentage of data remaining after removing data with a "bad" CI flag, the fourth after removing data with a "bad" CI flag and a broken-cloud flag. The last columns gives the percentage of data remaining after removal of data with a multiple-scattering flag.

Place + Wavelength	Total number of data points	CI-flag = good/med	CI-flag = good/med + no Broken Clouds	no Multiple Scattering
Xianghe 360 nm	29 740	56 %	43 %	61 %
Xianghe 477 nm	30 780	56 %	43 %	61 %
Brussels 360 nm	30 048	53 %	36 %	35 %
Jungfraujoch 360 nm	7693	78 %	53 %	54 %
Jungfraujoch 477 nm	7952	82 %	56 %	56 %

AMTD
7, 5883–5920, 2014

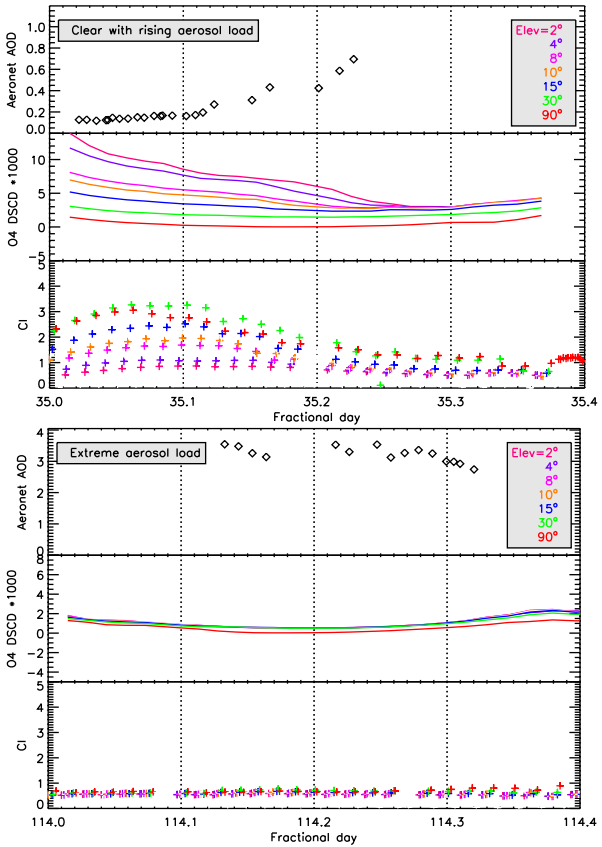

Figure 1. Comparison of four days at Xianghe with distinct meteorological conditions. The top box shows the measured AERONET AOD at 477 nm, the middle box the measured MAX-DOAS O_4 DSCDS and the bottom box the calculated colour index. Different colours represent the different MAX-DOAS elevation angles.

AMTD
7, 5883–5920, 2014

A simple and versatile cloud-screening method for MAX-DOAS retrievals

C. Gielen et al.

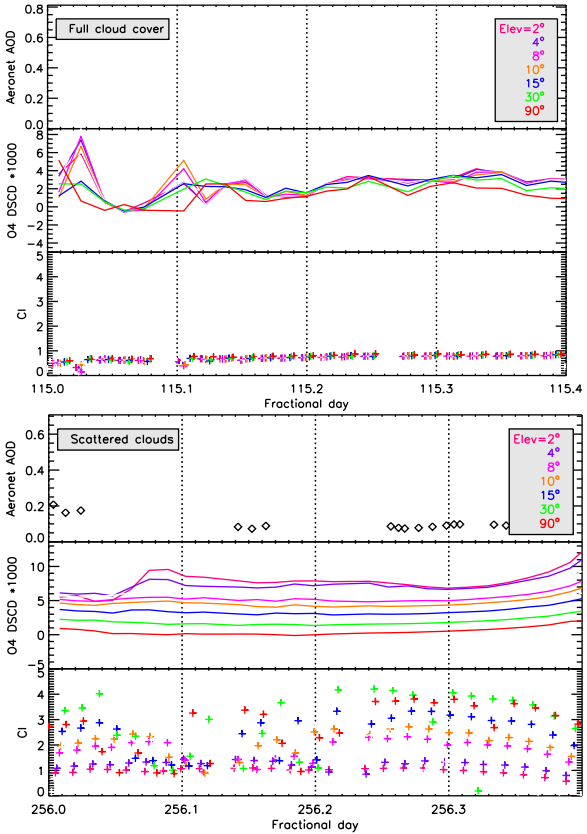

Figure 1. Continued.

AMTD
7, 5883–5920, 2014

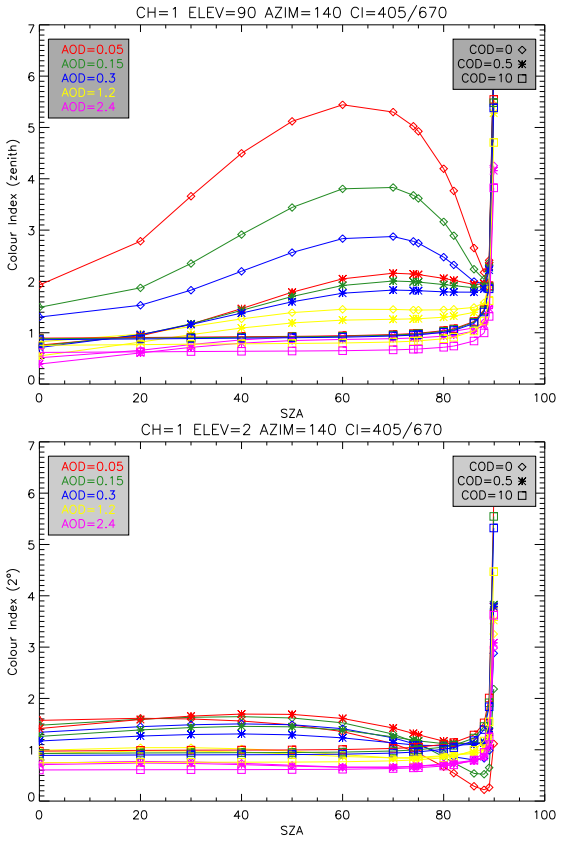

Figure 2. Simulations of the colour index under varying aerosol optical depth (AOD) and cloud optical depth (COD), and for two different elevation angles (Top: 90°/Bottom: 2°). The simulations were performed with the DAK plan-parallel radiative transfer model (Stammes, 2001), using a cloud-layer height of 1 km.

AMTD
7, 5883–5920, 2014

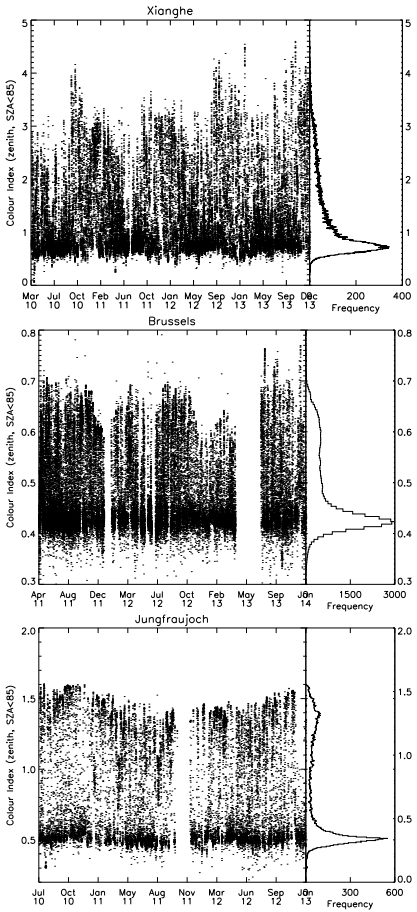

Figure 3. The calculated zenith CI values and frequency distribution for the full Xianghe, Brussels, and Jungfraujoch data sets.

AMTD
7, 5883–5920, 2014

A simple and versatile cloud-screening method for MAX-DOAS retrievals

C. Gielen et al.

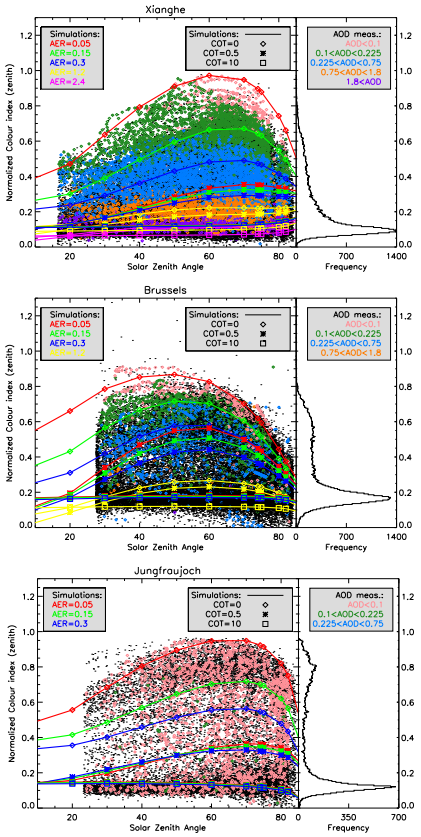

Figure 4. The normalized CI values (points) vs. solar zenith angle, together with the scaled CI simulations (coloured lines) made under different aerosol and cloud optical depth values (left/middle legend). We colour marked the observed CI values with additional AOD data if available (right legend).

AMTD
7, 5883–5920, 2014

A simple and versatile cloud-screening method for MAX-DOAS retrievals

C. Gielen et al.

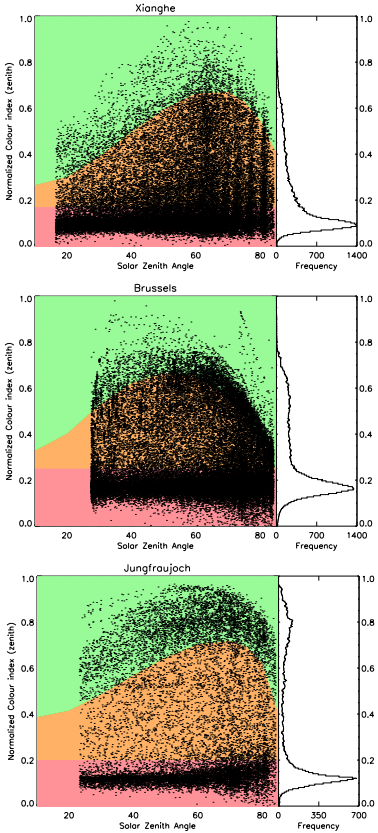

Figure 5. The normalized CI values (points) vs. solar zenith angle. The green, orange, and red regions correspond to the “good”, “mediocre”, and “bad” regions as defined by the sky flag.

AMTD
7, 5883–5920, 2014

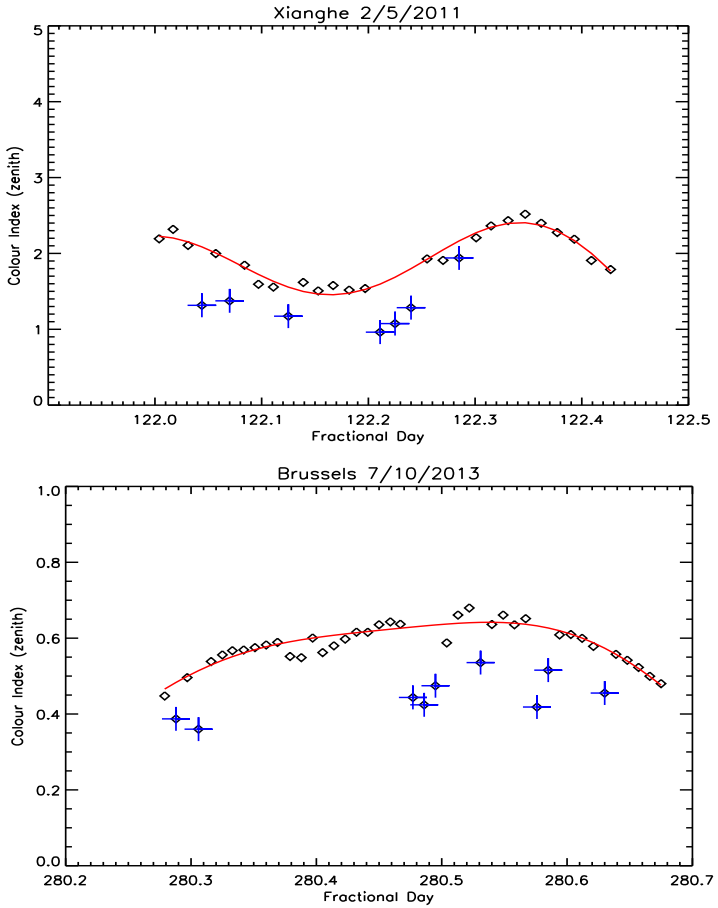

Figure 6. Results of the CI modelling (red line) to the calculated CI values (black diamonds) and outlier detection (blue crosses) for the broken-cloud flagging, for example days in Xianghe and Brussels.

AMTD
7, 5883–5920, 2014

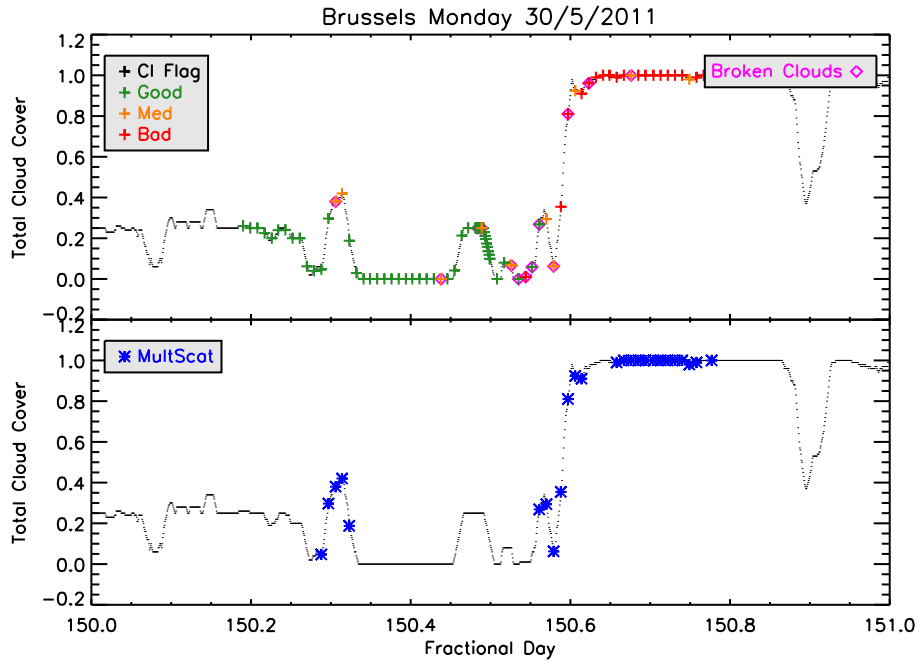

Figure 7. Total cloud-cover values from thermal infrared measurements are given in black points. Top: Overplotted in coloured crosses are the respective CI-flag values as derived from our cloud-screening method (green/orange/red = good/med/bad). Data with a broken-cloud flag is marked with a magenta diamond. Bottom: In blue asterisks we plot data points with a multiple-scattering flag.

AMTD
7, 5883–5920, 2014

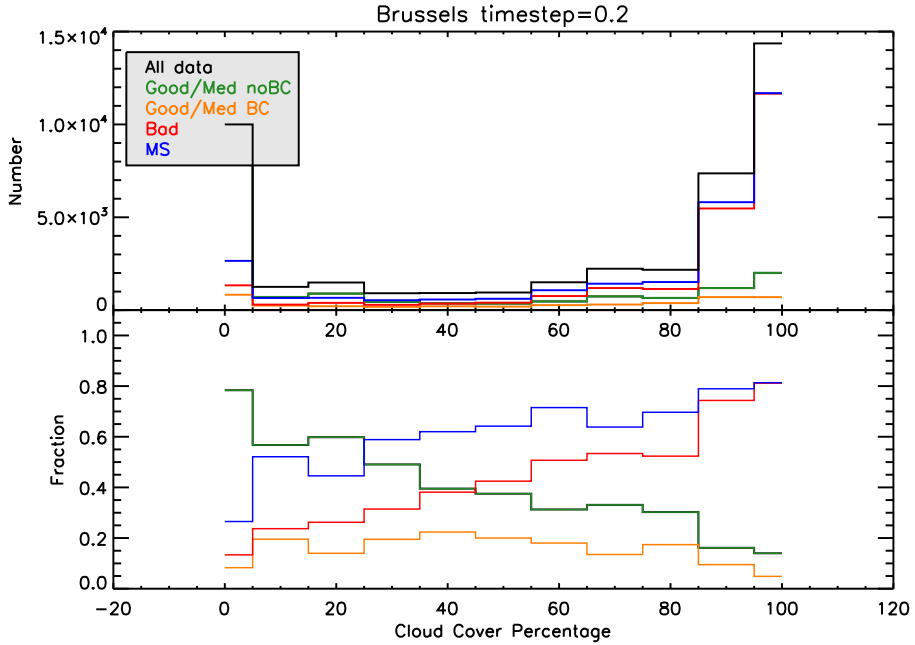

Figure 8. Top: Distribution of the cloud-cover percentages for the full Brussels data set in black, with the division of data points with different sky flags. In red we plot data with a "bad" sky flag, in orange data with a "good/med" sky flag and a broken-cloud flag, green denotes points with a "good/med" sky flag but no broken-cloud flag. In blue we mark data with a multiple-scattering flag. Bottom: Fraction of total cloud-cover values as distributed over our different flag values.

AMTD
7, 5883–5920, 2014

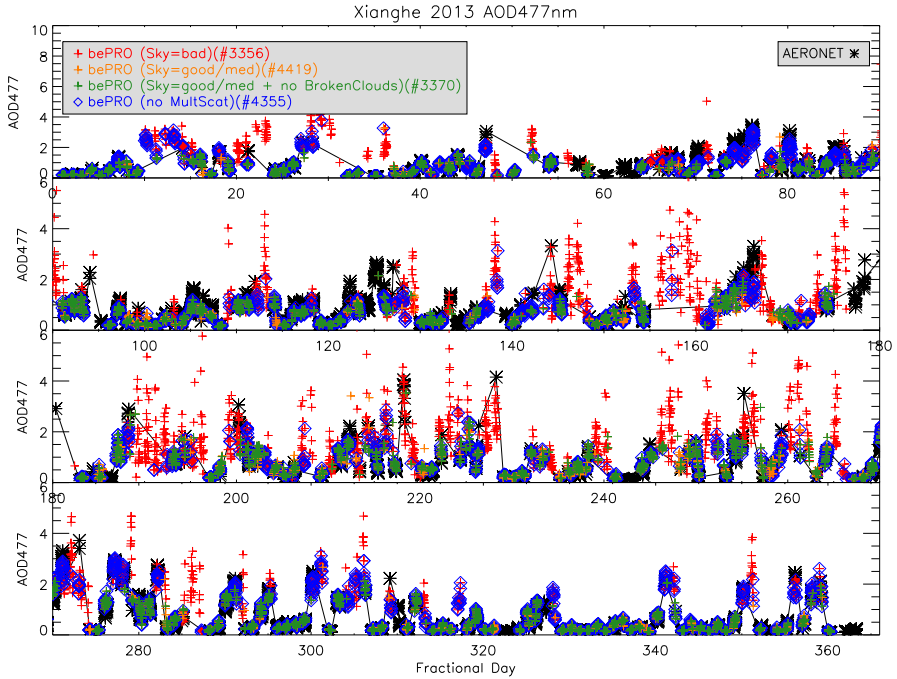

Figure 9. Example results of our bePRO AOD retrievals (crosses) compared to co-located AOD measurements (black diamonds). The different colours used for the retrievals denote the different cloud-screening results. Data with a "bad" sky flag are in red, data with a "good" or "mediocre" sky flag are in orange, data with a "good" or "mediocre" sky flag plus no broken-cloud flag are in green, and data with no multiple-scattering flag are in blue. More results can be found in the Supplement.

AMTD
7, 5883–5920, 2014

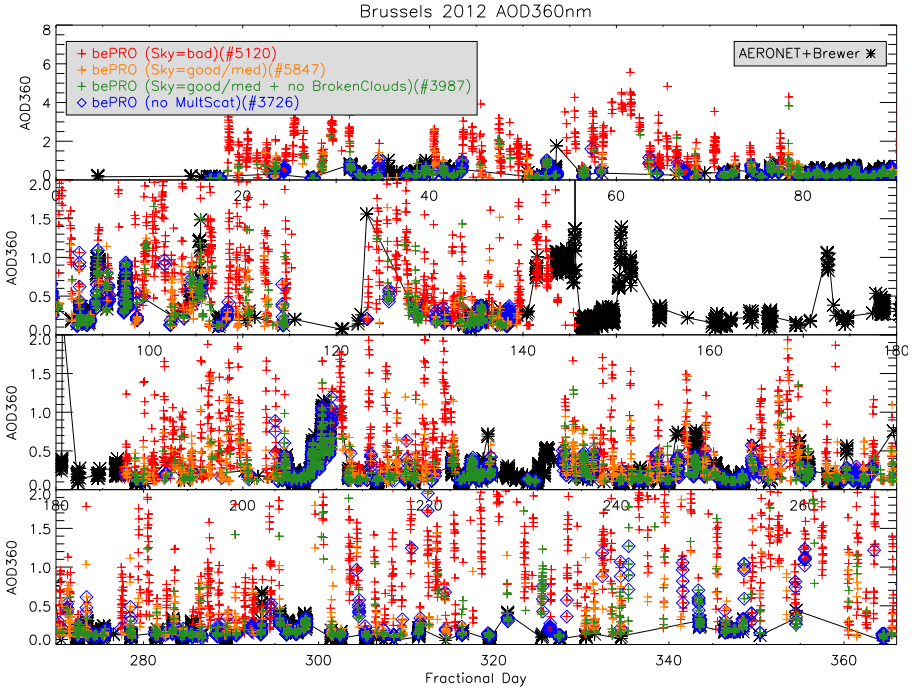

Figure 9. Continued.

AMTD
7, 5883–5920, 2014

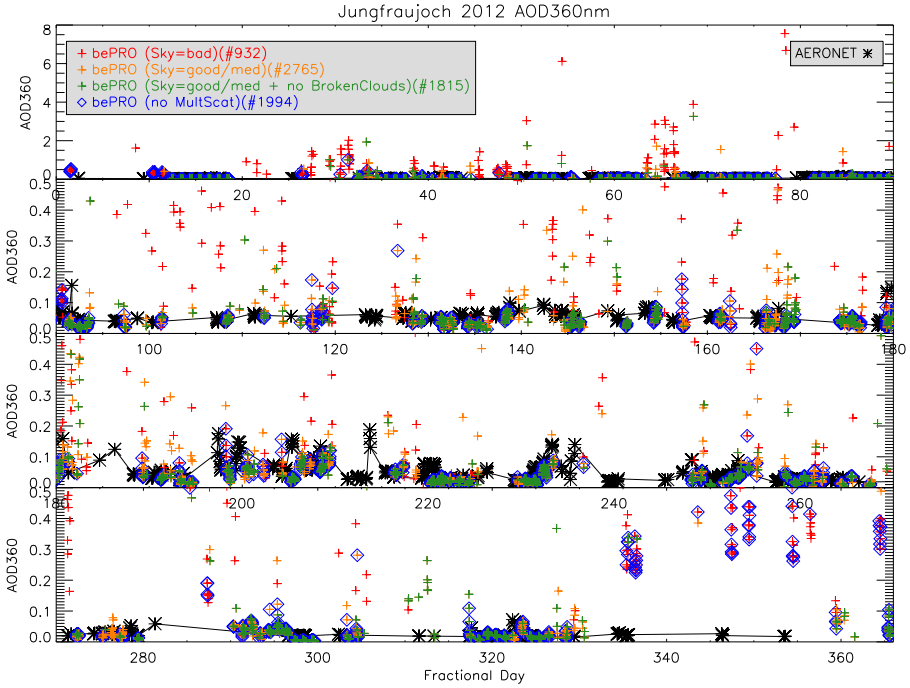

Figure 9. Continued.

AMTD
7, 5883–5920, 2014

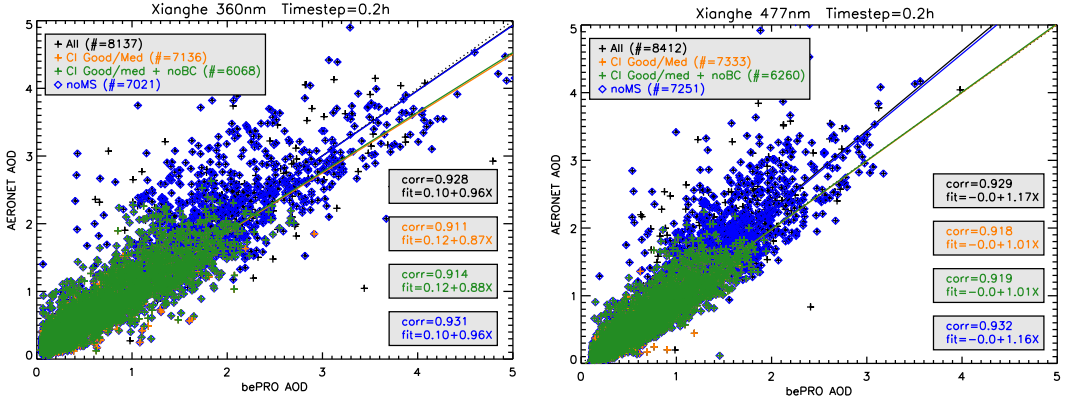

Figure 10. Correlation plots of our bePRO MAX-DOAS AOD retrievals and measured AOD values for the Xianghe and Jungfraujoch data set at 360 and 477 nm and for the Brussels at 360 nm, in time steps of 0.2 h. The full non-cloud-screening data is given by black crosses. Cloud-screened data (based on the CI) with a "good/mediocre" sky flag are marked in orange, data with "good/mediocre" sky flag and no broken-cloud flag are marked in green crosses. Data with no multiple-scattering flag (based on the O_4 DSCDs) are marked with blue diamonds. For each sample set we also give the linear regression lines and correlation information.

AMTD
7, 5883–5920, 2014

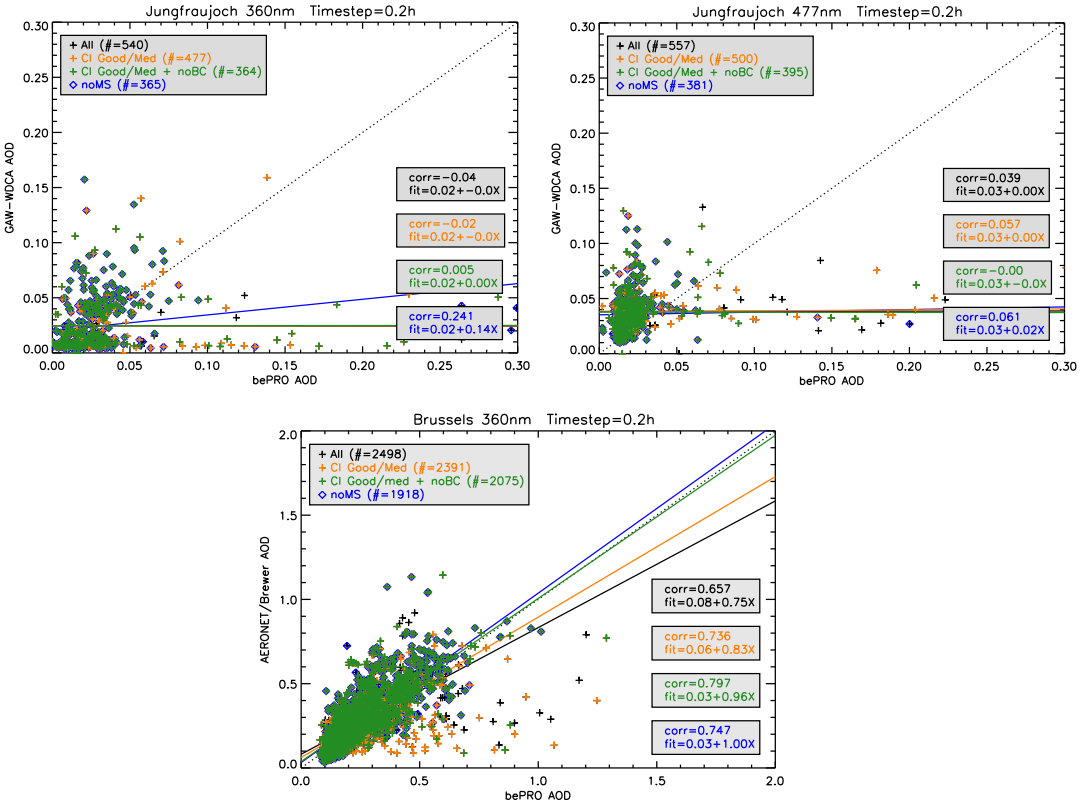

Figure 10. Continued.

AMTD
7, 5883–5920, 2014

A simple and versatile cloud-screening method for MAX-DOAS retrievals

C. Gielen et al.